NASA TECHNICAL NOTE

NASA TN D-4789

NASA TN D-4789

ADSORPTION-DESORPTION BEHAVIOR OF HOMOGENEOUS AND HETEROGENEOUS METAL SURFACES

by Thaine W. Reynolds

Lewis Research Center
Cleveland, Ohio

NATIONAL AERONAUTICS AND SPACE ADMINISTRATION • WASHINGTON, D. C. • SEPTEMBER 1968

NASA TN D-4789

ADSORPTION-DESORPTION BEHAVIOR OF HOMOGENEOUS AND HETEROGENEOUS METAL SURFACES

By Thaine W. Reynolds

Lewis Research Center
Cleveland, Ohio

NATIONAL AERONAUTICS AND SPACE ADMINISTRATION

For sale by the Clearinghouse for Federal Scientific and Technical Information
Springfield, Virginia 22151 – CFSTI price $3.00

ABSTRACT

Energy distribution relations which describe the desorption behavior from heterogeneous surfaces are presented. A graphical method of obtaining these is described, and the results are compared with a more exact computer-determined solution. Adsorption isotherms representing equilibrium coverage for the systems H_2-W, CO-W, N_2-W, CO-Mo, and N_2-Mo are presented covering a pressure range from 10^{-12} to 1 torr, a fractional surface coverage from 0.02 to 0.98 and for the appropriate temperature range in each case.

ADSORPTION-DESORPTION BEHAVIOR OF HOMOGENEOUS AND HETEROGENEOUS METAL SURFACES

by Thaine W. Reynolds

Lewis Research Center

SUMMARY

Equations and curves describing the adsorption of gas on metal substrates under equilibrium conditions, and the desorption of the gas from the surface under a linear temperature increase of the surface temperature are presented.

Results of an experimental investigation using the flash-filament desorption technique are used to obtain an energy-distribution relation for several gas-metal surface combinations. A graphical method of approximating the energy distribution relation which describes the desorption behavior from heterogeneous surfaces is presented and compared with the more exact solutions obtained on a digital computer. The range of the desorption energy spread was about 30 to 40 percent either side of the desorption energy value giving maximum desorption rate.

Systems for which quantitative experimental data are presented are hydrogen-tungsten, carbon monoxide-tungsten, nitrogen-tungsten, hydrogen-molybdenum, carbon monoxide-molybdenum, nitrogen-molybdenum, and hydrogen-tantalum. Some observations on the behavior of other gas-metal combinations are also made.

The energy distribution relation is then used to calculate adsorption isotherms. These isotherm plots express the equilibria expected over a range of pressures from 10^{-12} to 1 torr, for fractional surface coverages from 0.02 to 0.98 monolayers and for the appropriate temperature range in each case.

INTRODUCTION

Study of the adsorption and desorption behavior of gases on surfaces has become of considerable interest in recent years because of the availability and extended use of high vacuum equipment. In fact, the attainment of ultrahigh vacuum is usually accom-

plished by taking advantage of surface adsorption phenomena, such as in cryosorption and sublimation pumping.

Two simple "rules-of-thumb", which are frequently cited, serve to illustrate the relative importance of surface adsorbed species to the attainment of high vacua; they are the following:

(1) There may be 3×10^6 times as many particles on 1 square centimeter of an adsorbed monolayer as there are in 1 cubic centimeter of the gas phase at 10^{-8} torr.

(2) Gas molecules arrive at a surface at a rate equivalent to about one monolayer per second at 10^{-6} torr.

Consideration of the first point demonstrates that very small changes in surface coverage can involve enough particles to affect the pressure level of a system considerably.

The second point illustrates the necessity for working at very low pressures when studying "clean surface" phenomena.

In addition to the effect of adsorbed gas on vacuum system behavior, there are many surface phenomena that are greatly affected by the presence of adsorbed gas layers of a monolayer or less. Electron emission, surface ionization, surface diffusion, and catalysis are a few such phenomena.

One important experimental technique for studying surface adsorption and desorption behavior is that of flash-filament desorption (ref. 1). This technique involves the thermal desorption of adsorbed gases by heating the surface to high temperatures. However, work with the field emission microscope has pointed out that considerable surface migration of metals occurs at temperatures of one-third the melting point and lower (ref. 2). Thus, unless a surface which has been heated above this temperature level tends to reform to some equilibrium structure upon cooling, one would not expect to be investigating one particular surface structure. The temperatures required to clean a surface and to flash off chemisorbed material are, in general, considerably higher than the temperatures at which the surface may become quite mobile.

Considerable literature data are available for the flash filament desorption technique (ref. 1). The reproducibility of these data after successive flashes to high temperature levels must constitute some evidence for the return to an equilibrium surface structure on cooling. (Equilibrium, in this case, means only that the surface attains a structure which has repeatable desorption behavior.)

This report discusses adsorption isotherm relations and transient desorption behavior of energetically homogeneous and heterogeneous surfaces in general. It discusses the determination of site-energy relations for heterogeneous surfaces from experimental flash-filament desorption curves, and finally, presents some calculated adsorption isotherms which are based on the flash-filament-determined surface desorption energies.

The term, isotherm, is used herein to designate the relation between fractional surface coverage, surface temperature, and arrival rate or pressure.

THEORY

Equilibrium Adsorption-Desorption Isotherm Relations

Consider a surface immersed in a gas and at equilibrium with respect to adsorption and desorption of the gas.

The desorption rate of a gas from a constant energy surface is usually described by the relation (refs. 3 and 4).

$$\nu = \frac{\sigma^n}{\tau_{on}} e^{-E/kT_s} \tag{1}$$

where

ν desorption rate, particles/(cm^2)(sec)

σ surface coverage, particles/cm^2

n order of desorption relation

τ_{on} constant, sec

E desorption energy barrier, eV

k Boltzmann constant, eV/k

T_s surface temperature, K

(Symbols are defined in the appendix.)

The adsorption rate is generally expressed by defining a sticking coefficient S such that

$$\text{Adsorption rate} = \mu S \tag{2}$$

where μ is the arrival rate in particles per square centimeter per second.

At equilibrium the adsorption and desorption rates are equal, so that a simple isotherm relation becomes

$$\mu S = \frac{\sigma^n}{\tau_{on}} e^{-E/kT_s} \tag{3}$$

A more generally useful form for isotherm information has the coverage expressed explicitly as

$$\sigma = f(\mu, T_s) \tag{4}$$

Then, values for S, τ_{on}, n, and E must be known in order to use equation (3) to describe the adsorption data in the form of equation (4).

While the surface may be energetically uniform, E can vary with coverage because of interaction among the adsorbed particles. In the analytical treatment of uniform surfaces herein it will be assumed, as is usually done (e.g., ref. 3), that E does not vary with coverage. The value of τ_{o1} is sometimes treated as equal to h/kT_s or sometimes as the constant, 10^{-13} second. Also values of τ_{o1} and E may both be determined from plots of the experimental desorption data over a range of temperature. Each method may yield a different value of E. A discussion of the significance of the term, τ_o, may be found in reference 4.

Experimental values of E may be deduced readily from flash-filament desorption data as will be discussed shortly, but it should be kept in mind that the values reported depend on the equation used to obtain them. Desorption energy, per se, is not measured directly.

The reaction order n expresses the dependence of the desorption rate on the surface concentration of adsorbed molecules. The desorption rate of a monatomic gas or of a molecular gas which does not dissociate upon adsorption would be expected to depend directly on the surface concentration (i.e., $n = 1$). For a molecular gas which dissociates upon adsorption and recombines during desorption, the desorption rate would depend upon a higher order of surface concentration ($n > 1$). For most adsorbed species of interest, the reaction order n will be either 1 or 2 - or possibly some intermediate value if conditions are such that more than one desorption reaction is occurring simultaneously.

The sticking coefficient S is the remaining factor to be evaluated. It may vary with both temperature and surface coverage. Experimental values of S are required since there is no theoretical basis for calculating a value of sticking coefficient. Furthermore, there is considerable variation in reported values of sticking coefficient for the same systems.

For situations in which the temperature of the surface is above that corresponding to the saturation temperature of the gas, the adsorption amount is frequently found to approach a limiting coverage of a monolayer (ref. 5). One way of incorporating this limit into an isotherm relation is to assume that the sticking coefficient variation with coverage is simply

$$S = S_o(1 - \theta) \tag{5}$$

where $\theta = \sigma/\sigma_m$ and σ_m is the value for monolayer coverage. This is equivalent to assuming that particles arriving at filled adsorption sites are reflected.

Using this relation results in the isotherm equation (3) becoming

$$\mu(1 - \theta)S_o = \frac{\sigma^n}{\tau_{on}} e^{-E/kT_s} \tag{6}$$

This can be rearranged to yield the forms

$$\frac{\theta}{1 - \theta} = \mu S_o \frac{\tau_{o1}}{\sigma_m} e^{E/kT_s} \quad \text{for } n = 1 \tag{7}$$

and

$$\frac{\theta^2}{1 - \theta} = \mu S_o \frac{\tau_{o2}}{\sigma_m^2} e^{E/kT_s} \quad \text{for } n = 2 \tag{8}$$

Theoretical isotherm curves based on equations (7) and (8) are shown in figure 1 for a range of variables. Figure 1 has been made in the form of a nomograph for more compact presentation. In constructing these curves, values of $\tau_{o1} = 10^{-13}$ second and $\tau_{o2} = 50$ seconds per square centimeter were used. The value of τ_{o2} here is taken to be consistent with the ratio $\tau_{o2}/\tau_{o1} = \sigma_m/2$ determined from reference 6 and σ_m is taken as 1.0×10^{15} particles per square centimeter.

A nomograph relating arrival rate, pressure, temperature, and molecular weight is presented as figure 2 so that arrival rates needed for figure 1 are readily obtained for any particular gas. The relation used for figure 2 is

$$\mu = \frac{3.54 \times 10^{22}\, p}{\sqrt{T_g m}} \quad \text{molecules/(cm}^2\text{)(sec)} \tag{9}$$

where p is the pressure in torr and m is the molecular weight. The combination, μ/p, is used later in the report, and it should be noted that this expression is independent of pressure.

Transient Desorption Relations

Homogeneous surfaces. - One technique that has proved very useful for investigating the kinetics of desorption is the "flash-filament" method. The theory associated with this technique has been adequately presented in references 3, 7, and 8. The method consists of heating a surface, upon which a gas has been adsorbed, at a programmed rate, and noting the desorption rate as a function of temperature. Various time-temperature schedules are discussed in the references, but only one, a linear rate of temperature rise, will be considered here.

The desorption rate equation for the uniform surface is

$$\nu = \frac{\sigma^n}{\tau_{on}} e^{-E/kT_s} \tag{1}$$

Since the desorbing particles come only from the adsorbed layer

$$\nu = -\frac{d\sigma}{dt} \tag{10}$$

and equation (1) becomes

$$-\frac{d\sigma}{dt} = \frac{\sigma^n}{\tau_{on}} e^{-E/kT_s} \tag{11}$$

If a linear rate of temperature rise

$$\beta = \frac{dT_s}{dt} \tag{12}$$

is assumed, equation (11) can be expressed as

$$-\frac{d\sigma}{\sigma^n} = \frac{1}{\beta\tau_{on}} e^{-E/kT_s} dT_s \tag{13}$$

In order to integrate equation (13) the following approximation is found to be useful:

$$\frac{d}{dT_s}\left(T_s^2 e^{-E/kT_s}\right) = \frac{E}{k} e^{-E/kT_s}\left(1 + \frac{2}{E/kT_s}\right) \tag{14}$$

For the present situation, only values of $E/kT_s \geq 20$ will be of much interest, and the approximation that $2/(E/kT_s)$ is negligible compared to unity is made. With this approximation, equation (13) can be integrated to

$$\ln \frac{\sigma_0}{\sigma} = \frac{1}{\beta\tau_{o1}} \frac{k}{E}\left(T_s^2 e^{-E/kT_s} - T_{s0}^2 e^{-E/kT_{s0}}\right) \quad \text{for } n = 1 \tag{15}$$

and

$$\frac{1}{\sigma} - \frac{1}{\sigma_0} = \frac{1}{\beta\tau_{o2}} \frac{k}{E}\left(T_s^2 e^{-E/kT_s} - T_{s0}^2 e^{-E/kT_{s0}}\right) \quad \text{for } n = 2 \tag{16}$$

As long as $T_s \geq 1.1T_{s0}$, the T_{s0} term will be negligible with respect to the T_s term in equations (15) and (16). Dropping the T_{s0} terms and rearranging yield

$$\frac{\sigma}{\sigma_0} = \exp\left(-\frac{1}{\beta\tau_{o1}} \frac{kT_s^2}{E} e^{-E/kT_s}\right) \quad n = 1 \tag{17}$$

and

$$\frac{\sigma}{\sigma_0} = \frac{1}{1 + \frac{\sigma_0}{\beta\tau_{o2}} \frac{kT_s^2}{E} e^{-E/kT_s}} \quad n = 2 \tag{18}$$

Equations (17) and (18) are shown plotted in figure 3 for a range of variables E and T_s and for several values of β. Equations (17) and (18) describe the change in surface coverage, expressed as the ratio of coverage at any time (or temperature) to initial surface coverage σ/σ_0 for a surface whose temperature is increased at a constant rate. There is in general a narrow temperature range over which most of the desorption occurs for a constant energy surface. This range does not vary too greatly even for large changes in β, so that it is only necessary that the rate of temperature change of the surface be relatively constant over the portion of the temperature band

through which desorption occurs, to be able to interpret experimental desorption in terms of these theoretical curves.

It may be noted from equation (1) that, as temperature rises, the desorption rate increases. As desorption occurs, the adsorbed layer becomes depleted so that a maximum desorption rate finally occurs, after which the desorption rate drops as the temperature continues to rise. The desorption rate for the linear increase in temperature shows the typical trend illustrated in figure 4.

The theoretical temperature T_{max} at which the maximum desorption rate occurs is shown in figure 5 for both first- and second-order desorption, for a range of desorption energy values.

Heterogeneous surfaces. - Analysis of adsorption-desorption behavior for energetically heterogeneous surfaces - that is, surfaces for which E varies over the area independent of any variation that may be due to interaction between adsorbed particles - has been treated in references 3 and 7.

The desorption rate from such a surface is obtained by summing up the area-weighted rates of the separate patches with individual desorption energy E. If the distribution of energetic sites can be considered a continuum, then a site-energy distribution function f(E) can be used and the coverage ratio $\sigma(T_s)/\sigma_0$ for a heterogeneous surface can be expressed as

$$\frac{\sigma(T_s)}{\sigma_0} = \int_{E_1}^{E_2} f(E) \exp\left(-\frac{1}{\beta\tau_{o1}} \frac{kT_s^2}{E} e^{-E/kT_s}\right) dE \qquad n = 1 \tag{19}$$

or

$$\frac{\sigma(T_s)}{\sigma_0} = \int_{E_1}^{E_2} f(E) \left(1 + \frac{\sigma_0}{\beta\tau_{o2}} \frac{kT_s^2}{E} e^{-E/kT_s}\right)^{-1} dE \qquad n = 2 \tag{20}$$

These relations cannot generally be evaluated except for certain simple situations. Numerical methods of deducing the distribution function from experimental data and equations (19) and (20) must be employed as discussed in reference 7. A simple graphical method for approximating the distribution function is discussed in the next section of this report. A comparison of the results of this graphical method and the numerical solution is presented. Of course, the same restriction must be applied to the site-energy distribution relation as was put upon the desorption energy itself, namely, that

its values will depend upon the relations assumed to calculate it. The distribution may vary from one sample to another of the same metal.

Site-Energy Distribution

When a desorption trace for an initial coverage of a monolayer is available, a site-energy distribution characterizing the desorption can be determined. Assume a typical plot of experimental σ/σ_m against temperature superimposed on the set of desorption curves for a homogeneous surface as in sketch (a).

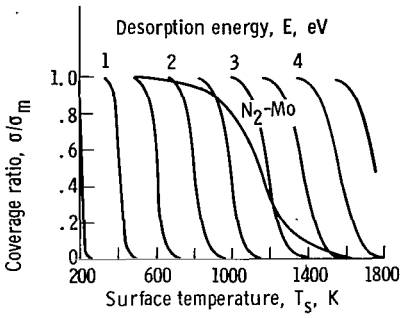

(a)

If the experimental range of temperatures and energies encompassing the complete desorption curve is broken up into a number of segments, a numerical solution to equation (19) or (20) can be obtained by writing a set of simultaneous linear equations. Equation (19) or (20), for instance, becomes

$$\sum_{E=E_1}^{E=E_2} f(E) \frac{\sigma(E, T_s)}{\sigma_m} \Delta E = \frac{\sigma(T_s)}{\sigma_m} \tag{21}$$

The right-hand terms of equation (21) are obtained from the experimental data curve. The $\sigma(E, T_s)/\sigma_m$ relation used is either equation (17) for $n = 1$ or equation (18) for $n = 2$.

A difficulty in the attempted solution of this set of simultaneous equations arose because of the exponential nature of the $\sigma(E, T_s)/\sigma_m$ terms. Negative values of some of the $f(E)$ terms would arise in order to satisfy the solution. These are, of course, physically meaningless in this instance. Herein, an iterative method of solution was used. The iterative process involved correcting the value of $f(E)$ for the E which gave the maximum desorption rate at the particular temperature. In this iterative

solution method, no negative f(E) values were permitted to occur. However, to obtain a reasonably smooth continuous solution may require use of a large number of segments. For the solutions presented herein, a 36×36 matrix of points was used. The resulting energy-distribution relation reproduced the experimental data curve to well within the accuracy of its initial determination.

It is also of interest to note that an approximation to the energy-distribution curve may be obtained directly from the graph of sketch (a). The method of doing so will be outlined here, and a comparison of this graphical method with the previous iterative solution will be shown in the RESULTS AND DISCUSSION section of this report.

Since the experimental curve of sketch (a) has been obtained for a monolayer coverage, the area fraction can be made to correspond with the coverage ratio. Furthermore, the relatively steep constant energy desorption curves give credence to the concept of the adsorption sites filling up and desorbing sequentially. It can be supposed then, that, since (in sketch (a)) no adsorption has occurred at about 500 K, there are no adsorption energy sites less than 1.5 electron volts. Similarly, since desorption is essentially complete by 1600 K, there are no sites with interaction energy greater than about 3.5 electron volts. Assuming the sequential filling up of sites, then, one can determine a value of F(E), the fraction of area which has a desorption energy equal or greater than any selected value E, by noting the value of E corresponding to σ/σ_m (in this case assumed equivalent to F(E)) along the experimental curve. A continuous curve of this area function against energy can be drawn (see sketch (b)).

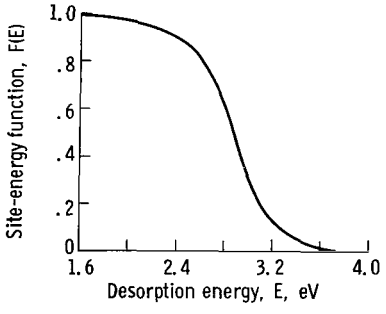

(b)

The site-energy distribution function f(E) and the function F(E) described previously are related by

$$f(E) = -\frac{dF(E)}{dE} \tag{22}$$

It might be helpful to examine the desorption curves obtained from some assumed site-energy distribution functions. Two such distributions are assumed: (I) - two equal areas of only two different energy sites, E = 2.5 and 4.5 electron volts, and (II) - three equal areas of just three energy sites, E = 2.5, 3.5, and 4.5 electron volts. Sketch (c) shows the appearance of the F(E) against E plots for these assumed distributions. In sketch (d) the corresponding comparative σ/σ_o against temperature curves that would be obtained from these distributions is shown.

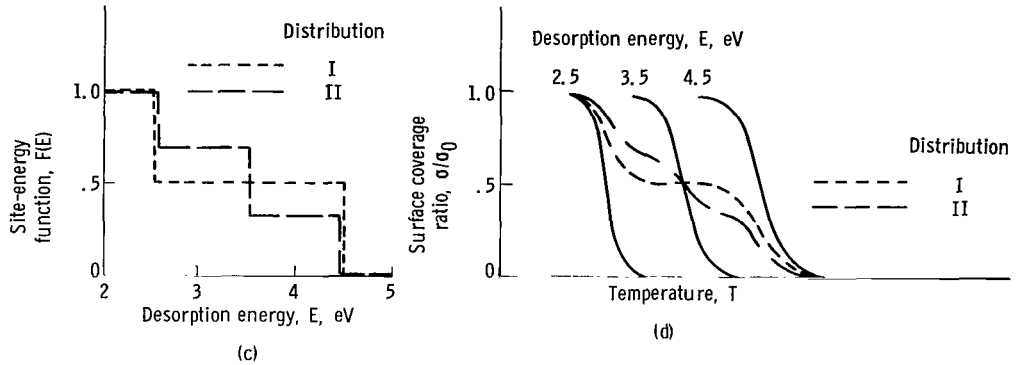

The trend is evident; as the fractional areas of the patches of any particular energy level decrease, the inflections in the σ/σ_o against temperature curve becomes less pronounced.

Isotherm Determination

Once a site-energy distribution relation for a particular gas-surface combination has been determined, the adsorption isotherms are readily calculable. If the distribution function were expressible analytically, the coverage fraction Θ would be obtained as

$$\Theta(T_s) = \frac{\int_0^\infty f(E)\theta(E, T_s)\, dE}{\int_0^\infty f(E)\, dE} \tag{23}$$

Herein, the total coverage fraction was evaluated numerically using the 36-point approximation to the relation f(E)

$$\Theta(T_s) \cong \frac{\sum_{i=1}^{36} f(E_i)\theta(E_i, T_s)\,\Delta E_i}{\sum_{i=1}^{36} f(E_i)\,\Delta E_i} \tag{24}$$

The values of $\theta(E, T_s)$ are obtained from equations (7) or (8) for $n = 1$ or 2, respectively.

EXPERIMENTAL APPARATUS AND PROCEDURE

A schematic layout of the apparatus used to obtain the experimental data reported herein is shown in sketch (e).

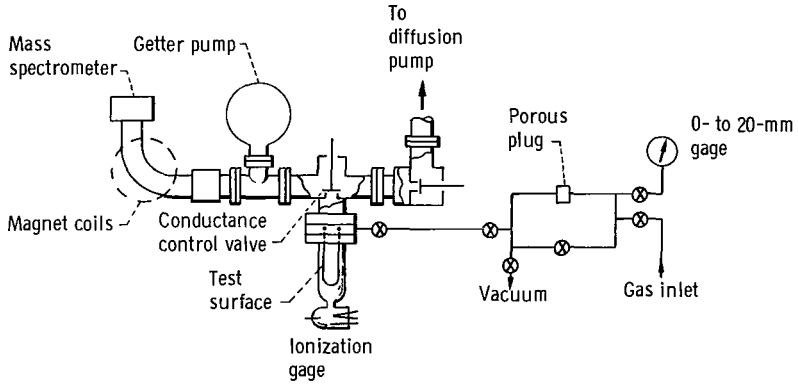

(e)

The test surfaces were wires 0.01 inch (2.54×10^{-4} m) or 0.005 inch (1.27×10^{-4} m) in diameter by 16 inches (0.406 m) long mounted inside a test volume of 1047 cubic centimeters. A T-valve between this chamber and the vacuum system permitted control of the conductance or pumping rate from the chamber. A Bayard-Alpert type ionization gage, operated at 0.1 normal emission level to reduce gage pumping effects, was used to measure test chamber pressure. Gas flow could be introduced to the chamber at controlled rates through a calibrated porous plug. A mass spectrometer was used to identify background constituents and desorbing species. All parts of the system were equipped with bakeout heaters.

The test filament was heated by a direct-current electric supply, which in turn was controlled by a motor driven transformer in order to achieve the desired temperature rise rate. The filament voltage and current readings, used to determine the wire temperature, were monitored continuously, along with ionization gage and mass spectrometer outputs, on a recording oscillograph.

Calibrations

The various volumes of the rig were determined. The porous plug was calibrated by measuring the rate of decrease of pressure in a known volume upstream of the plug. A typical plot is shown in sketch (f) for carbon dioxide (CO_2).

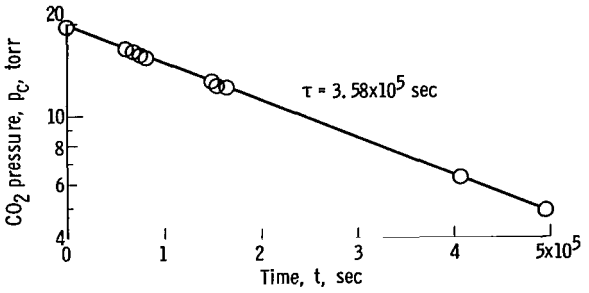

(f)

The plug was fabricated from 2 to 3-micron tungsten (W) powder so that the pore sizes were of this order of magnitude. The flow calibrations were made at pressures below 20 millimeter upstream pressure, at which level flow through this plug would be expected to be entirely within the free-molecule range (ref. 9).

The time constant τ was calculated from the relation

$$\frac{p_2}{p_1} = e^{-\Delta t/\tau} \tag{25}$$

For free-molecule flow, the constant for a system can be derived as

$$\tau = 2.73 \times 10^{-4} \frac{V}{C_A} \sqrt{\frac{m}{T_g}} \quad \text{sec} \tag{26}$$

and is seen to be proportional to $\sqrt{m}$.

A plot of the time constants obtained for nitrogen (N_2), hydrogen (H_2), and helium (He) confirm the $\sqrt{m}$ dependence for this plug in the range used (sketch (g)).

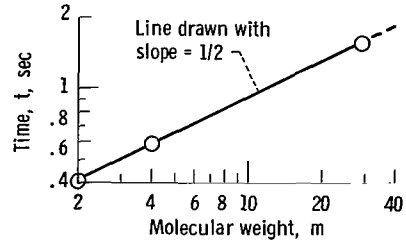

(g)

The conductance of the T-valve which is needed to obtain quantitative desorption rates, was determined in terms of the ion gage readings for several gases. A flow rate was set through the porous plug, and the ion gage was then read for various settings of the T-valve. This was repeated for several flow rates. A typical plot of these readings for N_2 is shown in sketch (h).

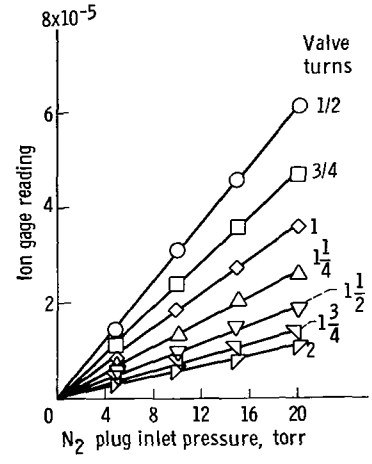

(h)

From curves such as these then, the flow rate through the T-valve can be determined for any setting of the valve and reading of the ion gage. It should be noted that the absolute gage factor of the ion gage, which would be needed to obtain true system pressures, need not be known to obtain true flow rates in this case. Only if one now wishes to determine flow rate through the T-valve for some gas for which a primary calibration was not obtained will it be necessary to know the relative gage factor for that gas compared to one used in the calibrations.

The wire temperature was determined from its resistance using the resistivity data of reference 10 for tungsten and reference 11 for molybdenum (Mo) and tantalum (Ta). Temperatures in the higher temperature range were checked initially using an optical pyrometer and also by comparing experimental power requirements against calculated radiant energy loss from the wire. All methods were found to be in excellent agreement. A calculation of the expected temperature distribution over the length of the wire was made following the relations noted in reference 12. The cooling effects on the wire ends caused by conduction to the supports reduces the area which is uniform in temperature (i.e., to within experimental accuracy) to about 95 percent of the wire length.

Procedure

A typical procedure to obtain a desorption trace was as follows. The wire was flashed to clean its surface, after which it was returned to room temperature. Gas pressure was established at some specified pressure level and adsorption allowed to occur for a certain length of time, herein called "adsorption time". The T-valve was then opened to a setting for which the transmission area had been determined. During this time, the system pressure would become established at a value designated p_{eq}.

The temperature of the wire was then increased at a specified temperature rise rate β to a temperature level at which the particular gas would be all desorbed. The pressure and temperature curves as functions of time were followed during this desorption step. Simultaneous mass traces were also taken during desorption to identify the desorbing gas.

These data were then analyzed in the manner outlined in the next section.

Data Analysis

Consider the system shown schematically in sketch (i) which incorporates the essential features of the experimental apparatus.

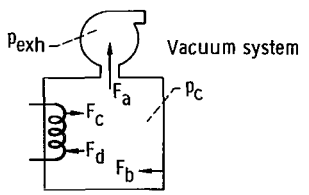

(i)

A mass flow balance on the system yields

$$\frac{dN}{dt} = F_c - F_d + F_b - F_a \tag{27}$$

where

N total number of atoms in chamber

F_c desorption rate from test surface, particles/sec

F_d adsorption rate onto test surface, particles/sec

F_b combined flow rate into chamber from all sources other than test surface (i.e., leak, outgassing, intentionally introduced flow, etc.), particles/sec

F_a net flow rate out of chamber to pump, particles/sec

These various flows are determined as follows:

$$F_a = \frac{\mu}{p} C_A(p_c - p_{exh}) \tag{28}$$

where C_A is the equivalent area of a sharp-edged orifice which has the same conductance as the system has through the opening to the vacuum pump. The rate F_a will either be set at some predetermined value or be known from calibration procedures. Then

$$F_c = \nu A_s \tag{29}$$

and

$$F_d = \mu S A_s \tag{30}$$

where A_s is the surface area, herein used as πdL where d is wire diameter and L is wire length. Substituting equations (28), (29), and (30) into equation (27) yields

$$\frac{dN}{dt} = \nu A_s - \mu S A_s + F_b - \frac{\mu}{p} C_A(p_c - p_{exh}) \tag{31}$$

By using the ideal gas law, equation (32) is put in terms of pressure as

$$\frac{dp}{dt} = \frac{kT_g}{V}\left[\nu A_s - \mu S A_s + F_b - \frac{\mu}{p} C_A(p_c - p_{exh})\right] \tag{32}$$

This relation (eq. (32)) describes the behavior of pressure in the test volume under the combined actions of adsorption and desorption from the test surface, introduced gas flows, and continuous pumpout of gas from the chamber. Interpretation of the system behavior for several different ways of operating will be apparent using equation (32).

In determining the transmission area of the T-valve C_A for instance, a steady flow rate of gas was introduced. This rate is much greater than any leak or outgassing rate, so that F_b is equal to the known introduced rate in this case. The pressure reached an equilibrium value p_{eq} so that $dp/dt = 0$. The surfaces reach equilibrium with respect to adsorption and desorption rates; that is,

$$\nu A_s = \mu S A_s \tag{33}$$

Thus,

$$F_b = \left(\frac{\mu}{p}\right) C_A (p_{eq} - p_{exh}) \tag{34}$$

or

$$C_A = F_b \left(\frac{p}{\mu}\right)\left(\frac{1}{p_{eq} - p_{exh}}\right) \tag{35}$$

Now consider the desorption trace in sketch (j), which might be typical of the pressure-time behavior in the system under continuous temperature increase of the surface, with continuous pumpout.

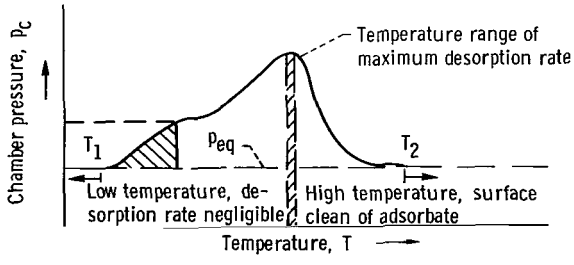

(j)

Since F_b in equation (32) represents the combined flows of introduced gas and background leaks and outgassing rates, equation (34) applies whenever the surface is at equilibrium with respect to adsorption and desorption rates and $dp/dt = 0$. Substitution of equation (34) into equation (32) yields

$$\frac{dp_c}{dt} = \frac{kT_g}{V}\left[\nu A_s - \mu S A_s - C_A \frac{\mu}{p}(p_c - p_{eq})\right] \tag{36}$$

The rate at which particles are removed from the system over and above the rate F_b as a result of continuous temperature increase of the test surface is given by

$$\frac{dN}{dt} = C_A \frac{\mu}{p}(p_c - p_{eq}) \tag{37}$$

Since it is assumed that these particles only come from the test surface and that readsorption is negligible during the desorption phase, the total integral under the pressure-time curve above p_{eq} yields the total initial surface coverage

$$\sigma_0 A_s = \int_0^{\infty} \frac{\mu}{p} C_A (p_c - p_{eq})\, dt \equiv \int_{t_1}^{t_2} \frac{\mu}{p} C_A (p_c - p_{eq})\, dt \tag{38}$$

At some intermediate time, the number of particles that have been desorbed involves the area under the curve up to that point in time, plus a contribution which consists of the particles that have been desorbed but not yet pumped out. This latter term is

$$\Delta N_{\substack{\text{desorbed but} \\ \text{not pumped}}} = \frac{V}{kT_g}(p_c - p_{eq}) \tag{39}$$

Thus at time t,

$$\sigma(t) A_s = \sigma_0 A_s - \int_0^t \nu A_s\, dt \tag{40}$$

Using equation (38) results in

$$\sigma(t) A_s = \int_{t_1}^{t_2} \frac{\mu}{p} C_A (p - p_{eq})\, dt - \int_{t_1}^{t} \frac{\mu}{p} C_A (p - p_{eq})\, dt - \frac{V}{kT_g}(p - p_{eq}) \tag{41}$$

The pressure-time curve during desorption may be analyzed by means of equation (41) to yield a surface concentration-temperature relation, which may then be compared with the theoretical curves of figure 3. If the pumping rate through the T-valve is

sufficiently rapid in comparison to the desorption rate, then the temperature at which the pressure reaches a maximum corresponds closely to the temperature at which the maximum desorption rate occurs (ref. 3). For the conditions of this experiment, the maximum difference between these two temperatures is about 2 percent according to the analysis of reference 3.

RESULTS AND DISCUSSION

Results are presented for each particular metal surface investigated and for each gas for which data were obtained with that metal. Site-energy distributions calculated from these data are presented. Finally, some calculated isotherms are presented using these site-energy relations.

Adsorption-Desorption Data

Generally after bakeout of the system and heating of the wire filaments to a high temperature level (2800 K for tungsten and 2500 K for molybdenum and tantalum), the background gas composition consisted mainly of H_2, He, water (H_2O), and carbon monoxide (CO). In no instance in the tests herein was any He or H_2O desorption noted from the test surfaces.

A series of curves, typical of those obtained with most systems, will be shown only for the first gas-surface combination presented. Data for the remainder of the systems will be summarized in table I or in the figures.

Tungsten. - Tungsten is the easiest metal on which to obtain a clean surface since it can be heated to a higher temperature than any other metal without melting or subliming.

Hydrogen: Desorption of hydrogen from tungsten is shown in sketch (k) for a H_2 background pressure of 7.8×10^{-10} torr during adsorption. The area under these curves is proportional to the initial surface coverage. The surface coverage buildup that occurred is shown in sketch (ℓ).

The maximum desorption rate is seen (in sketch (k)) to occur at lower temperatures as the initial coverage increases. This behavior is typical of a second-order desorption for constant E surfaces as is illustrated by the theoretical curves of figure 5(b). A plot of the values of this maximum temperature T_{max} for this data and for another similar set of H_2-W data is shown in figure 5(b). The general level of the desorption energy is seen to be 1.7 to 2.0 electron volts assuming a second-order desorption. Table II contains a summary of some literature values (ref. 1) with which results on the

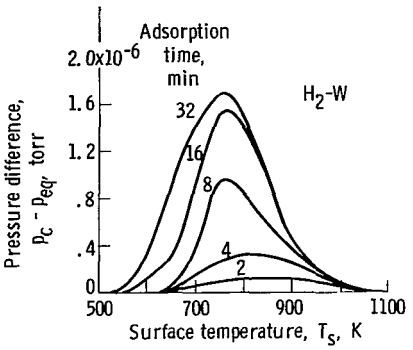

(k)

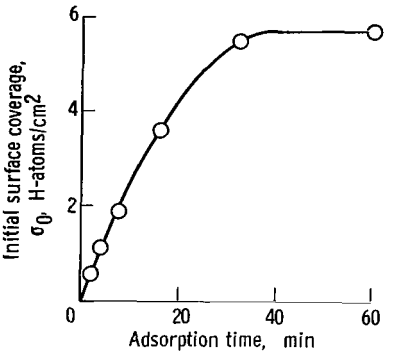

(l)

various systems reported herein may be compared.

A typical desorption curve obtained after adsorption at hydrogen pressures up to 10^{-5} torr is shown in figure 6 along with other typical curves. The maximum surface coverage obtained in these tests was 1.0×10^{15} H-atoms per square centimeter. This value is taken as monolayer coverage for the H_2-W system. The data curve of figure 6 was used to determine the site-energy distribution relation for the H_2-W system in the manner previously described.

Carbon monoxide: The maximum amount of adsorbed CO on tungsten measured was 5.3×10^{14} CO-molecules per square centimeter. Figure 6 shows the desorption trace for this maximum coverage case. Since CO apparently does not dissociate on adsorption (ref. 13), the temperatures of maximum desorption rate for this system are plotted on the first-order theoretical plot (fig. 5(a)). The general level of desorption energy for the CO-W system is seen to be 3.3 to 3.4 electron volts.

Carbon monoxide desorption curves obtained both from adsorption of background CO gas and from introduction of CO_2 into the system which dissociated on adsorption. There was no difference in desorption characteristics of the CO between the two cases.

Nitrogen: Desorption of nitrogen from tungsten is also shown in figure 6 for the maximum surface coverage of 6.44×10^{14} N-atoms per square centimeter. The temperatures of the maximum desorption rate obtained for the N_2-W system are plotted in figure 5(b). The desorption energy level is 3.7 to 4.1 electron volts.

Other gases: Carbon dioxide and oxygen were also introduced into the system but no quantitative adsorption data were obtained with these gases on tungsten. Qualitatively, the following behavior was observed. It appears that CO_2 is dissociated readily on contact with the tungsten surface, even at low temperatures (i.e., near ambient). This has been discussed elsewhere (ref. 13). A small amount of CO_2 desorbed as such at temperatures around 500 K. The remaining adsorbed material desorbed as CO. The excess oxygen may either have reacted with carbon already in the metal, coming off as CO, or remained to desorb as O or oxygen (O_2) at higher temperature levels. Similarly,

no quantitative data were obtained on O_2 desorption. The only qualitative reproducible behavior noted was a desorption peak which coincided with the 32 mass line and occurred in the temperature range 2340 to 2440 K. If the kinetics for desorption are first order, a desorption energy of 6 to 6.3 electron volts is indicated (fig. 5(a)). If the desorption is second order, the desorption energy could range down to around 5.5 electron volts (fig. 5(b)). Since coverage was not determined, the actual value of σ_o/β could not be determined.

Molybdenum. - Molybdenum cannot be heated to quite as high a temperature as tungsten. Nevertheless, it can still be cleaned of most species by high temperature treatment. It has been reported (ref. 14) that CO adsorbed on molybdenum cannot be removed by high temperature treatment below the melting point of molybdenum. Data presented in the following sections are in contradiction to this statement.

Hydrogen: Temperatures at which the maximum desorption rate occurred with the H_2-Mo system are shown plotted in figure 5(b). If second-order desorption is assumed, the energy level is 1.35 to 1.55 electron volts.

The maximum amount of adsorbed H_2 measured was 2.65×10^{14} H-atoms per square centimeter. This maximum measured amount here is undoubtedly not monolayer coverage, but more probably was close to the equilibrium value expected in the system at the existing H_2 pressure and temperatures. Without being able to take the surface temperature below ambient in this experimental setup, it is impossible to reach and maintain monolayer coverage. Even though higher coverages may be reached by raising the H_2 pressure, the areas of lower desorption energy will rapidly desorb during the time interval in which the system pressure is being lowered prior to starting a desorption trace. So, while the adsorption of hydrogen on molybdenum could be followed over some of the area, desorption from a complete monolayer could not be observed in this experiment.

Carbon monoxide: The temperature at which the maximum desorption rate occurred for the CO-Mo system did not vary with the initial adsorbed amount. This is typical of the expected behavior of first-order desorption from monoenergetic surfaces. The values of T_{max} are consequently shown on the theoretical first-order graph (fig. 5(a)) and show the desorption energy level to be about 3.1 to 3.3 electron volts.

The desorption trace for the maximum coverage case, 4.83×10^{14} CO-molecules per square centimeter, is shown in figure 6. This number is treated as monolayer concentration herein for the CO-Mo system.

Nitrogen: A desorption trace for the maximum coverage case for nitrogen on molybdenum is shown in figure 6. The coverage, 1.16×10^{15} N-atoms per square centimeter, is taken as the monolayer value for this system. A plot of the temperature for maximum desorption rates, shown in figure 5(b), yields the general level of desorption energy of 3.0 electron volts for N_2-Mo.

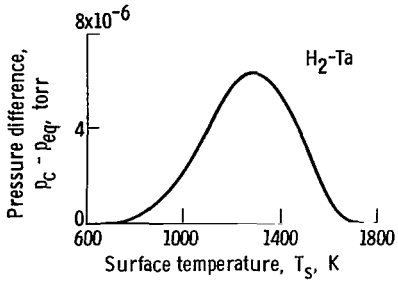

(m)

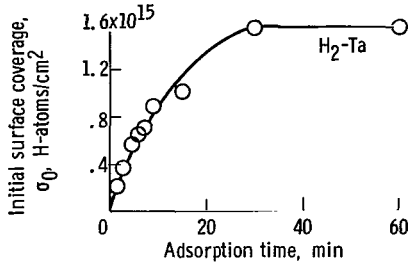

(n)

Mercury: Several attempts to measure adsorption of mercury on molybdenum yielded no indication of adsorption in the range above room temperature. This was surprising in view of the results reported in reference 15, which indicate adsorbed amounts at temperatures up to 650 K, a readily measurable condition in the present experiment. The fact that no measurable adsorption was noted at room temperature would indicate a range of desorption energies for the Hg-Mo system below about 1.0 electron volt (see fig. 3). Reference 15 cites a desorption energy value of 1.8 electron volts.

Tantalum. - Tantalum exhibited adsorption behavior quite different from that of tungsten or molybdenum. While tantalum can be heated to as high, or higher, a temperature than molybdenum, the adsorbed gases are not as readily desorbed.

Hydrogen: At a hydrogen pressure of 5×10^{-9} torr, the desorption curves of H_2-Ta were similar to those obtained on Mo or W, except that the temperature level was considerably higher. A typical trace is shown in sketch (m). The temperature of the maximum desorption rate is plotted in figure 5(b) for several such traces. The general desorption energy level from this data is 2.9 to 3.1 electron volts assuming second-order desorption.

A plot of the buildup of surface concentration with adsorption time at an H_2 pressure of $\sim1\times10^{-8}$ torr is shown in sketch (n). A maximum coverage of 1.56×10^{15} H-atoms per square centimeter under these conditions was measured. This number is in the range that might be considered monolayer coverage, though it is higher than anticipated. However, when hydrogen pressures up to 10^{-5} torr were introduced, the subsequent desorption curves yielded amounts of desorbed H_2 much in excess of this "monolayer range" value. In fact, desorbed H_2 equivalent to nearly 50 times this value was measured. Even this was not necessarily a limiting value, but further pressurization was not done. It seems that this excessive amount of hydrogen must be penetrating into the interior of the tantalum metal. However, the temperature of maximum desorption rate showed a decreasing trend with "coverage" as shown in sketch (o). This trend seems peculiar in that, if hydrogen were penetrating into the metal lattice, the subsequent time required for the H_2 to reach the surface before desorbing would be expected to show up as as a higher maximum temperature level in the desorption trace. A desorption energy of

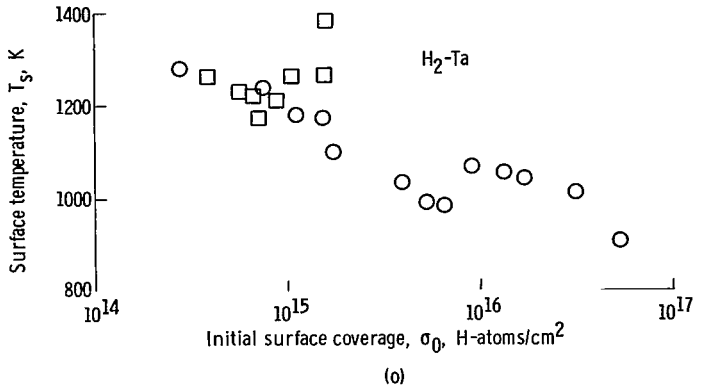

(o)

2.82 electron volts is reported for this system by Krakowski (ref. 16). He also suggests H_2 solubility in bulk tantalum as a possible explanation of some of his observed behavior.

Other gases: It was of interest to see if the adsorption characteristics of deuterium were the same as H_2 on tantalum. The temperature range of desorption and the temperature of maximum desorption rate for a number of desorption traces indicated that D_2 behavior was the same as H_2 with tantalum. T_{max} values of 1250±100 K were obtained for over a dozen desorption traces, indicating the D_2-Ta desorption energy level to be around 2.8 to 3.2 electron volts.

Carbon monoxide desorption from tantalum started at a temperature level of around 1900 K, but never reached a maximum desorption rate for wire temperatures up to about 2800 K.

No N_2 desorption was observed from Ta, even though adsorption pressure levels as high as 10^{-4} torr were used.

The fact that CO desorption was never complete, and no nitrogen desorption observed indicates that the tantalum surface was probably never very clean. Then, the hydrogen and deuterium desorption cited previously is probably from some Ta-X surface.

Site-Energy Determination

The experimentally determined curves of surface coverage ratio σ/σ_m against temperature are shown in sketches (a) and (p).

These experimental curves for completely covered monolayers for the systems CO-W, CO-Mo, H_2-W, N_2-Mo, and N_2-W were used to calculate energy-area relations as previously outlined. The results of these calculations are shown in figure 7.

Also shown in these figures are the F(E) curves which were determined directly from the graphical plots (sketches (a) and (p)). It is apparent that the graphical approach outlined yields a reasonable approximation to the computer-determined distribution,

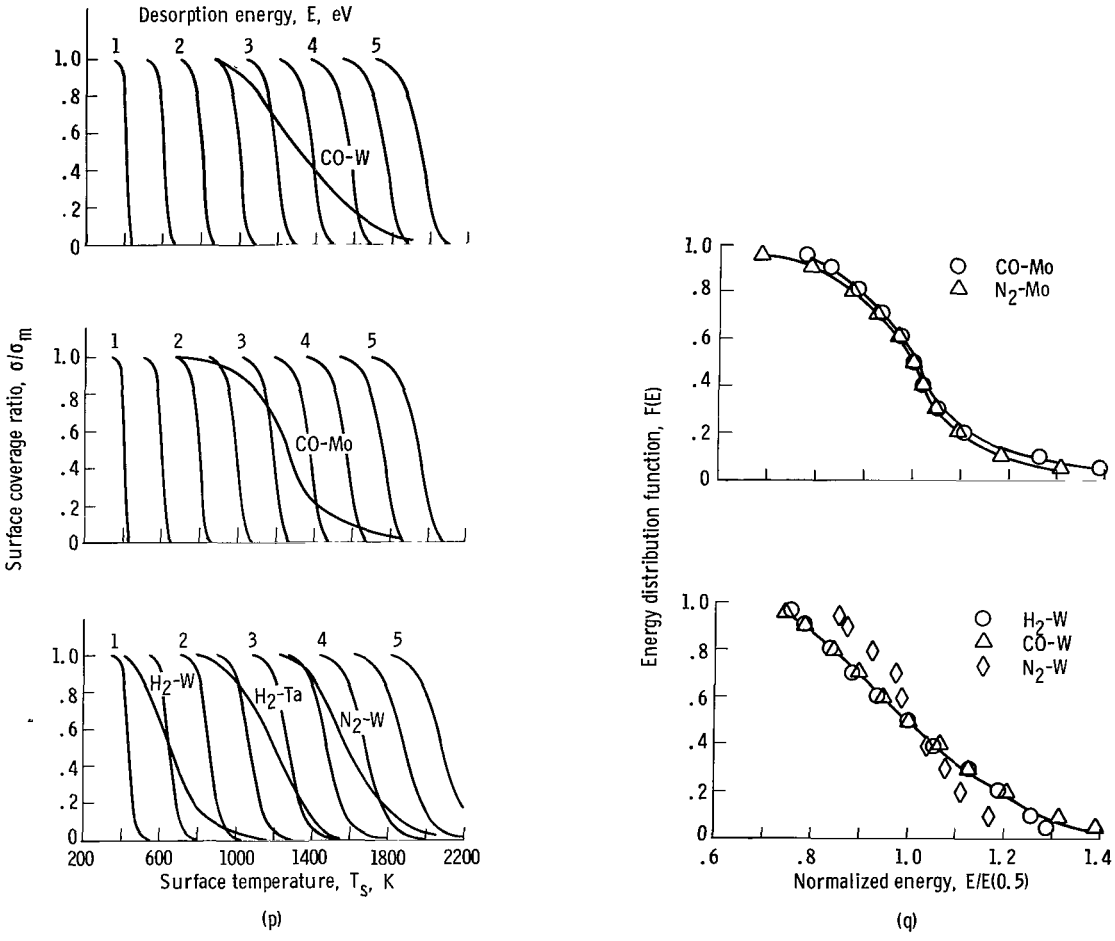

except for the case of the N_2-W data. For these cases, at least, the graphical approach yields a slightly narrower energy spread than the computer solution. As was mentioned previously, the effect of plateaus in the F(E) against E curves may not be readily apparent in the desorption traces. It is not certain that the inflections in the energy distribution curve for the N_2-W system are representative of the gas-surface interaction energy entirely for that system, or are affected by the sensitivity of the particular numerical calculation. The resulting isotherm calculations will not be greatly influenced by small variations in the site-energy distribution vurves.

This experiment alone is not capable of distinguishing between variations in $E(\Theta)$ due to interactions between adsorbed particles and the variations due to surface heterogeneity. In order to see if there were any similarities in desorption behavior that might be attributed to surface variation alone, the F(E) curves of figure 7 were plotted with the energy scale normalized to the E-value at half coverage (sketch (q)). The shapes of these curves are different for molybdenum and tungsten, but do have similarity between different gases on the same surface, which is at least suggestive of a given surface-

patch distribution. The N_2-W data again are not consistent in this comparison.

The general spread in desorption energies for these cases is seen to be from about 30 percent below to about 40 percent above the energy at half coverage.

Isotherm Determination

Sticking coefficient. - For conditions of negligible desorption rate, the sticking coefficient is defined as follows:

$$\text{Adsorption rate} = \mu S \tag{2}$$

The time derivative of the surface coverage (for instance, the slope of the curve in sketch (ℓ) or (o)) can give values of S. If, at the values of coverage and temperature involved, the desorption rate is not negligible, then the determination of S from experimental data must include the desorption rate term in the relation; that is,

$$\text{Adsorption rate} = \mu S - \nu \tag{42}$$

Since ν is a relatively sensitive function of T_s and E, as well as coverage, it is obviously less accurate to determine a value of sticking coefficient under these conditions.

Generally, the sticking coefficient is calculated through equation (2) even though the conditions of negligible desorption rate may not be met. This is done because the experiment frequently simply does not yield the attendant values of ν to use. This leads to "pseudosticking" coefficients which drop to zero at coverages of less than unity.

Sticking coefficients determined from data presented herein are shown in sketch (r). The solid lines are plots of the relation $S = S_o(1 - \theta)$, with $S_o = 0.37$ for N_2-W, 0.17 for H_2-Ta, and 0.22 for H_2-W. (Comparative values of S from the literature are also given in table II).

There is considerable variation in values of S in the literature for a given system (see ref. 17, for example). Some probable reasons for the variations are also cited therein. A wide variation in sticking coefficient with crystal face has been reported for the H_2-W system (ref. 18). Presence of impurity gases can cause error in the measurements. In view of the relative uncertainty of sticking coefficient values, the isotherm calculations presented here were made using only the clean surface value of sticking coefficient S_o. Variation with coverage is assumed to follow equation (6). The trend of values of S shown in sketch (r) as well as other reported values (ref. 17)

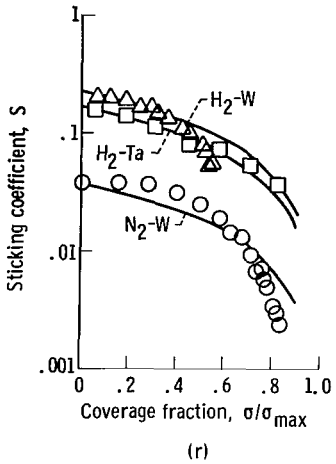

(r)

indicates this to be a reasonable assumption. The assumption is the same as that used in calculating the generalized isotherm plots of figure 1.

Calculated isotherms. - Isotherm data calculated for the same systems are shown in figure 8. These isotherms were determined using the computer-determined f(E) relations and equation (24). Other data necessary to calculate these plots are included in table I. Pressure range selected for these plots was from 10^{-12} to 1 torr with the appropriate temperature range to yield fractional coverages from 0.02 to 0.98.

Lines of constant total coverage Θ did plot as straight lines on the log p against 1/T plots. Thus, a constant value of desorption energy $E(\Theta)$ can be used to express the total desorption rate from the heterogeneous surface at any given total coverage value. The values of $E(\Theta)$ determined from the slopes of these lines are shown in figure 7 also for comparison. Curves for $E(\Theta)$ against Θ are plotted in figure 9.

The graphical method of obtaining the F(E) against E relation produces values that may be used to describe the distribution relation and to calculate adsorption isotherms. It appears that, if the true F(E) is a reasonably continuous function of energy, the resulting calculations using the graphical F(E) relation will be a good approximation to the presumably more correct computer values.

CONCLUDING REMARKS

Equations and curves describing the adsorption of gas on metal substrates under equilibrium conditions, and the desorption of gas from the surface under a steady temperature increase of the surface temperature have been presented.

Results of an experimental investigation using the flash-filament desorption technique are presented. Gas-metal surface combinations for which quantitative experi-

mental data are presented are: hydrogen-tungsten, carbon monoxide-tungsten, hydrogen-molybdenum, carbon monoxide-molybdenum, nitrogen-molybdenum, and hydrogen-tantalum. Some observations on the behavior of other gas-metal combinations were also made.

The experimental data were treated to yield energy-distribution functions for the gas-metal combinations. A simplified graphical method of approximating the energy-distribution function was presented. This method gave values which can be used to obtain adsorption isotherms in good agreement with the computer-determined values.

Adsorption isotherms were calculated using the experimentally determined energy-distribution relations. These isotherm plots along with the monolayer coverage value σ_m express the expected equilibrium amount of gas adsorbed over a range of pressures from 10^{-12} to 1 torr, surface coverages from 0.02 to 0.98 monolayers, and for the appropriate temperature range in each case.

Lewis Research Center,
National Aeronautics and Space Administration,
Cleveland, Ohio, June 6, 1968,
129-01-02-07-22.

APPENDIX

SYMBOLS

A_s	surface area, cm^2
C_A	transmission area, cm^2
d	wire diameter, cm
E	desorption energy, eV (1 eV ≡ 1.6×10^{-19} J)
F_a	net flow out of test chamber, particles/sec
F_b	combined flow into test chamber, particles/sec
F_c	desorption rate, particles/sec
F_d	adsorption rate, particles/sec
F(E), f(E)	site-energy distribution functions
$f(\mu, T_s)$	function of μ and T_s
h	Planck's constant, J-sec
k	Boltzmann constant, eV/K
L	wire length, cm
m	molecular weight
N	number of molecules
n	order of reaction
p	pressure
p_c	chamber pressure, torr
p_{eq}	equilibrium pressure in test chamber
p_{exh}	pressure of exhaust chamber
S	sticking coefficient
S_o	sticking coefficient at zero coverage
T	temperature
t	time
V	volume
β	rate of temperature increase of surface, dT/dt, K/sec

Θ overall fractional monolayer coverage of heterogeneous surface

θ fractional monolayer coverage, σ/σ_m, of homogeneous patch

μ arrival rate, particles/(cm^2)(sec)

ν desorption rate, particles/(cm^2)(sec)

σ surface coverage, particles/cm^2

σ_m monolayer surface coverage, particles/cm^2

σ_0 initial surface coverage, particles/cm^2

τ time constant in eq. (20), sec

τ_{on} constant in n^{th}-order desorption equation, sec

τ_{o1} constant in first-order desorption equation, sec

τ_{o2} constant in second-order desorption equation, sec

Subscripts:

g gas

i i^{th} component of area

max maximum

s surface

1,2 initial and final states of process

REFERENCES

1. Swanson, L. W.; Bell, A. E.; Hinrichs, C. H.; Crouser, L. C.; and Evans, B. E.: Literature Search of Physical Property Data and of Composite Surface Work Function Models. Field Emission Corp. (NASA CR-85562). Dec. 15, 1966.

2. Müller, Erwin W.: Surface Migration of Tungsten on a Single Crystal Lattice. Zeit. f. Phyzik, vol. 126, 1949, pp. 642-665.

3. Redhead, P. A.: Thermal Desorption of Gases. Vacuum, vol. 12, no. 4, July-Aug. 1962, pp. 203-211.

4. DeBoer, J. H.: Adsorption Phenomena. Advances in Catalysis. Vol. VIII. W. G. Frankenburg, V. I. Komarewsky, and C. K. Rideal, eds., Academic Press, 1956, pp. 17-161.

5. Langmuir, Irving: Phenomena, Atoms and Molecules. Philosophical Library, New York, 1949, p. 53.

6. Glasstone, Samuel; Laidler, Keith J.; and Eyring, Henry: The Theory of Rate Processes. McGraw-Hill Book Co., Inc., 1941.

7. Carter, G.: Thermal Resolution of Desorption Energy Spectra. Vacuum, vol. 12, no. 5, Sept.-Oct. 1962, pp. 245-254.

8. Ageev, V. N.; Ionov, N. I.; and Ustinov, Yu. K.: The Use of Pulse Mass Spectroscopy for Investigating Adsorption Characteristics by the Flash Method. Soviet Phys.-Tech. Phys., vol. 9, no. 3, Sept. 1964, pp. 424-432.

9. Reynolds, Thaine W.; and Kreps, Lawrence L.: Gas Flow, Emittance, and Ion Current Capabilities of Porous Tungsten. NASA TN D-871, 1961.

10. Weast, Robert C., ed.: Handbook of Chemistry and Physics. 45th ed., Chemical Rubber Co., 1964-1965, p. E-110.

11. Kohl, Walter H.: Handbook of Materials and Techniques for Vacuum Devices. Reinhold Publ. Co., 1967.

12. Jain, S. C. and Krishnan, S. K.: The Distribution of Temperature Along a Thin Rod Electrically Heated in Vacuo. I. Theoretical. Proc. Roy. Soc., Ser. A, vol. 222, no. 1149, Mar. 9, 1954, pp. 167-180.

13. Hayward, D. O.; and Gomer, Robert: Adsorption of Carbon Dioxide on Tungsten. J. Chem. Phys., vol. 30, no. 6, June 1959, p. 1617.

14. Parry, A A.; and Pryde, J. W.: Adsorption of Nitrogen and Carbon Monoxide on Molybdenum. Brit. J. Appl. Phys., vol. 18, 1967, pp. 329-334.

15. Bennette, C. J.; Strayer, R. W.; Swanson, L. W.; and Cooper, E. C.: Behavior of Various Adsorbates on Metal Substrates. Field Emission Corp. (NASA CR-54704), Feb. 18, 1966.

16. Krakowski, Robert A.: Dissociation of Hydrogen on Tantalum Using Modulated Molecular Beam Technique. Rep. UCRL-17336, Univ. California, Mar. 1967.

17. Lewin, Gerhard S.: Fundamentals of Vacuum Science and Technology. McGraw-Hill Book Co., Inc., 1965.

18. Armstrong, R. A.: The Reflection of Slow Electrons by Hydrogen-Covered Single Crystals on Tungsten. Can. J. Phys., vol. 44, no. 8, Aug. 1966, pp. 1753-1764.

19. Gavrilyuk, V. M.; and Medvedev, V. K.: The Adsorption of Barium Atoms and Carbon Monoxide Molecules on the (113) Face of a Tungsten Single Crystal. Soviet Phys.-Solid State, vol. 4, no. 9, Mar. 1963, pp. 1737-1744.

20. Pasternak, R. A.; and Wiesendanger, Hans U. S.: Interaction of Hydrogen and of Nitrogen With a Molybdenum Ribbon. J. Chem. Phys., vol. no. 6, June 1961, pp. 2062-2068.

TABLE I. - SUMMARY OF PARAMETERS

System	Maximum coverage, σ_{max}, cm^{-2}	Clean surface sticking coefficient, S_o	Temperature of maximum desorption rate, T_{max}, K	Desorption energy associated with maximum rate, E, eV	Reaction order, n
H_2-W	1.0×10^{15} H-atoms	0.22	740 to 860	1.7 to 2.0	2
N_2-W	6.44×10^{14} N-atoms	.037	1500 to 1700	3.7 to 4.1	2
CO-W	5.3×10^{14} CO-molecules	[a].5	1370 to 1430	3.3 to 3.4	1
N_2-Mo	1.16×10^{15} N-atoms	[b].7	1180 to 1220	3.0	2
CO-Mo	4.83×10^{14} CO-molecules	[c]1.0	1220 to 1270	3.1 to 3.3	1
H_2-Ta	[d]1.58×10^{15} H-atoms	.17	1170 to 1280	2.9 to 3.1	2
H_2-Mo	[e]2.65×10^{14} H-atoms	.24	570 to 700	1.35 to 1.55	2

[a]Ref. 19.

[b]Ref. 20.

[c]Estimated in lieu of experimental value.

[d]Not maximum coverage, see text.

[e]Not believed maximum attainable.

TABLE II. - DESORPTION ENERGY, STICKING COEFFICIENT, AND MONOLAYER COVERAGE FOR SOME GAS-METAL SYSTEMS

[All values as cited in ref. 2, but only those of interest above 300° are cited.]

System	Desorption energy, E, eV	Clean surface sticking coefficient, S_o	Monolayer surface coverage, σ_m, particles/cm^2
H_2-W	1.35, 2.9, 1.48±0.07, 1.10, 1.26, 0.87 to 2.0	0.1, 0.2 0.1 (100 plane) 0.3 (211 plane) ~0.01 (111 plane) <10^{-3} (110 plane)	7.5×10^{14}
N_2-W	3.5	0.3 to 0.4	3×10^{14} to 10×10^{14}
CO-W	α_1, 0.87 to 1.26[a] β_1, 2.26 to 2.74[a] β_2, 3.02 to 3.35[a] β_3, 3.28 to 4.35[a]	0.2, 0.49, 0.50, 0.48	4.5×10^{14} to 9.5×10^{14}
H_2Mo	----------	0.35	8.2×10^{14}
N_2-Mo	----------	0.6, 0.7	4.4×10^{14}

[a]Designations α and β are as used in ref. 2.

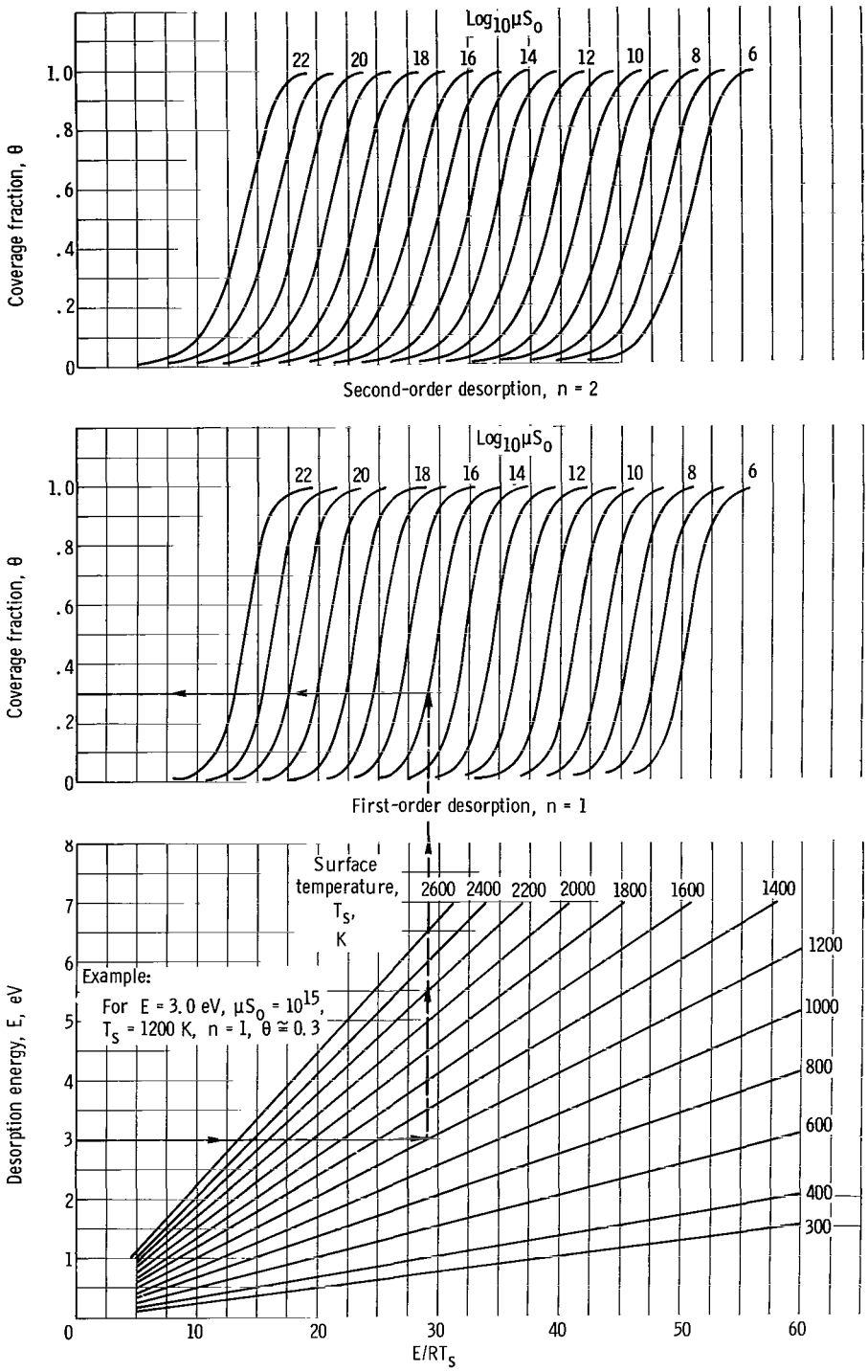

Figure 1. - Variation of equilibrium surface coverage with arrival rate and surface temperature for surfaces of constant desorption energy. First- or second-order desorption.

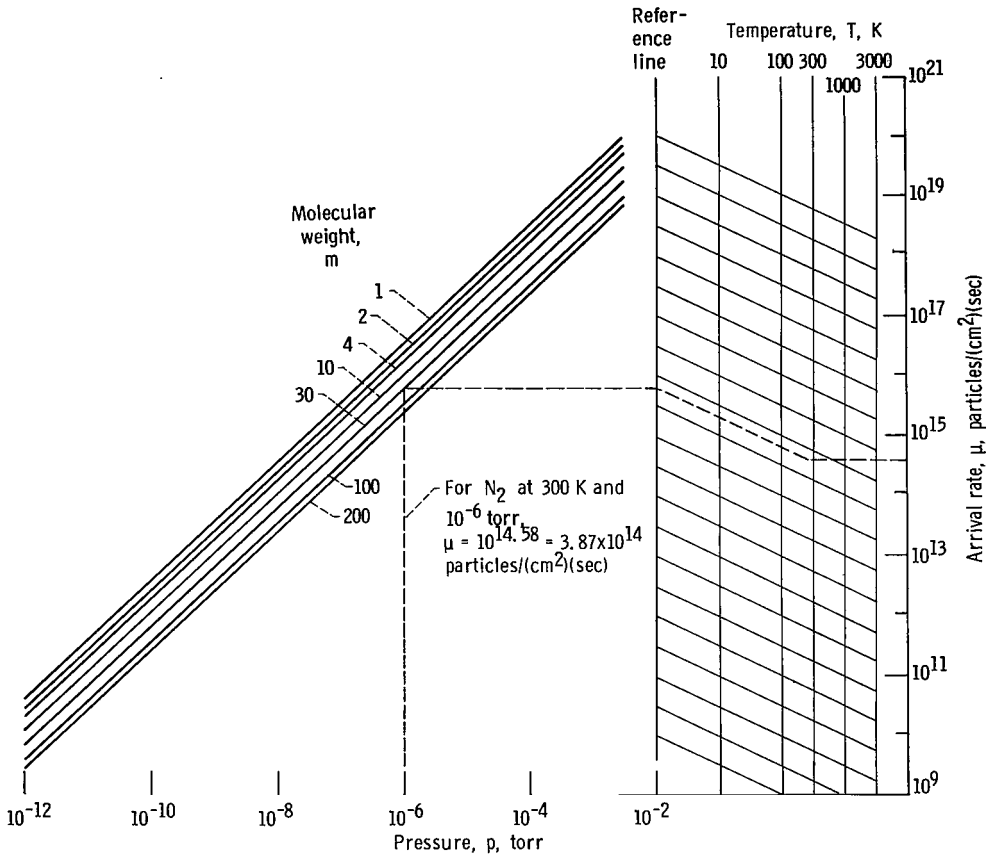

Figure 2. - Nomogram of arrival rate equation.

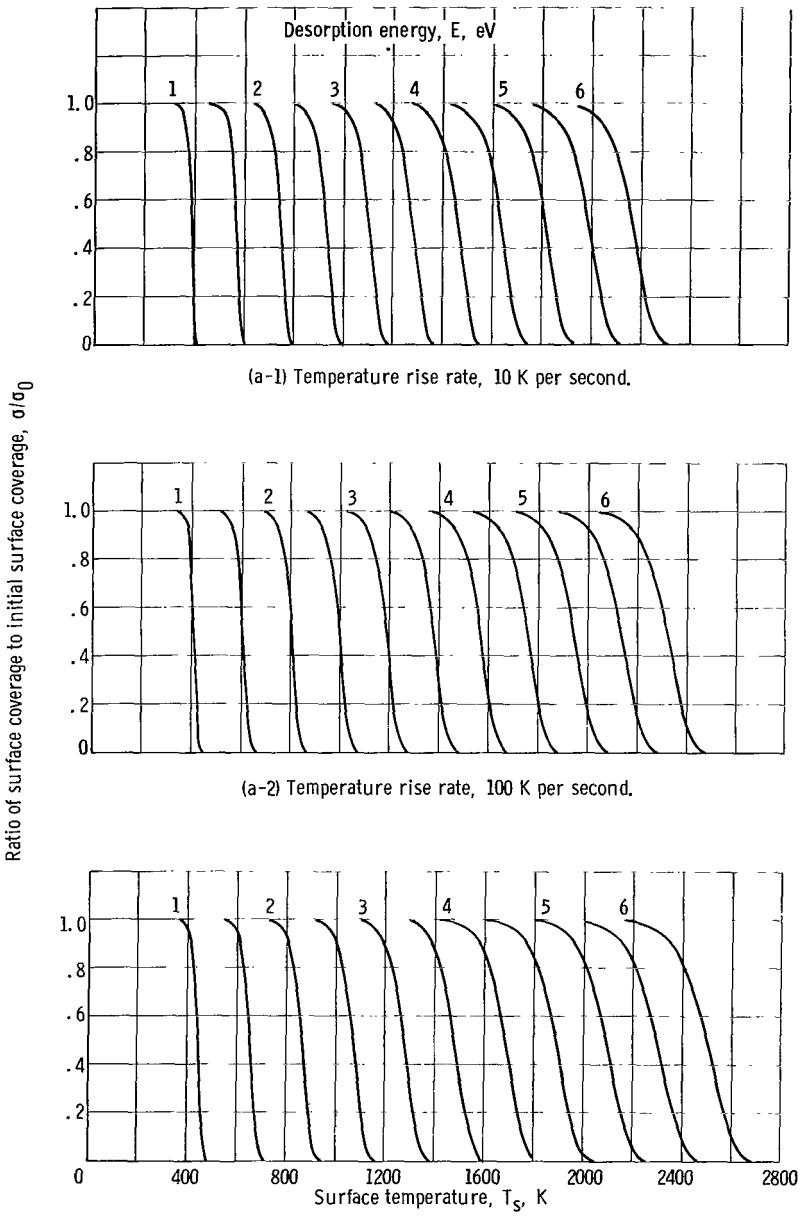

(a-1) Temperature rise rate, 10 K per second.

(a-2) Temperature rise rate, 100 K per second.

(a-3) Temperature rise rate, 1000 K per second.

(a) First-order desorption, $n = 1$; $\tau_{01} = 10^{-13}$

Figure 3. - Variation of surface coverage with surface temperature during desorption of constant energy surface at various temperature rise rates.

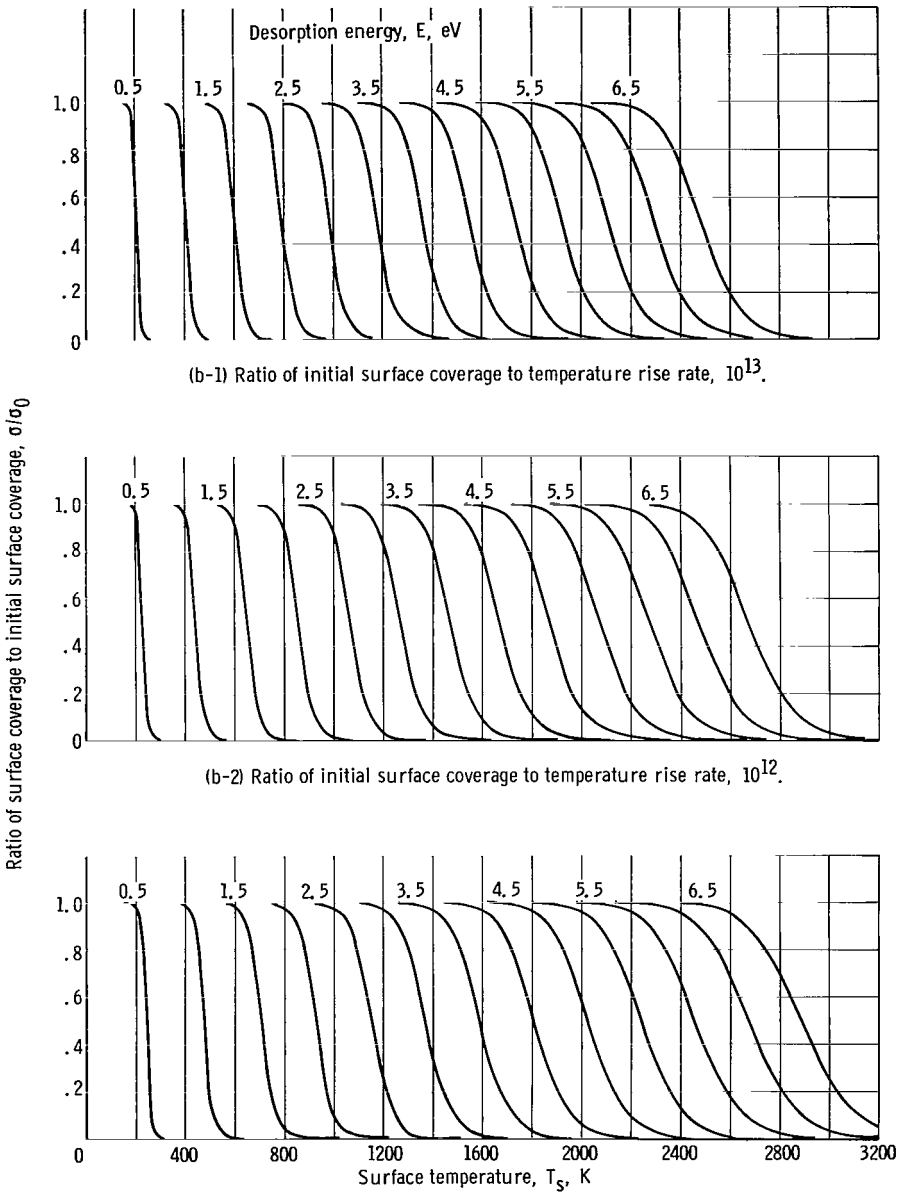

(b-1) Ratio of initial surface coverage to temperature rise rate, 10^{13}.

(b-2) Ratio of initial surface coverage to temperature rise rate, 10^{12}.

(b-3) Ratio of initial surface coverage to temperature rise rate, 10^{11}.

(b) Second-order desorption, $n = 2$; $\tau_{02} = 50$.

Figure 3. - Concluded.

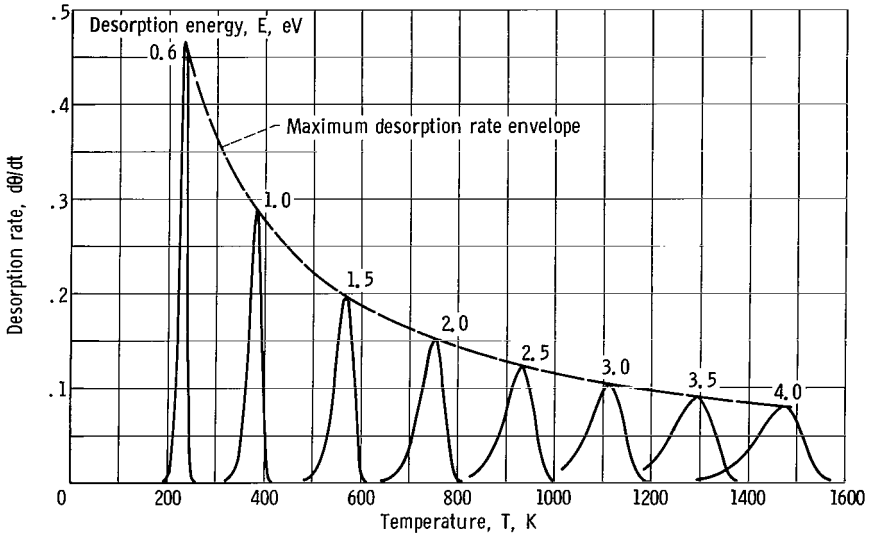

Figure 4. - Variation of desorption rate with temperature during desorption of constant energy surface. First-order desorption temperature rise rate, 10 K per second.

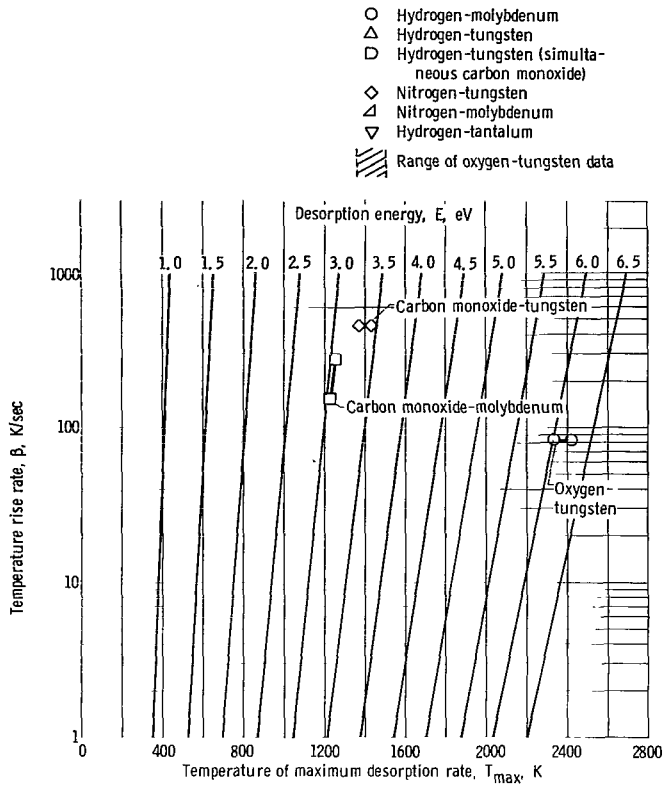

(a) First-order desorption, n = 1.

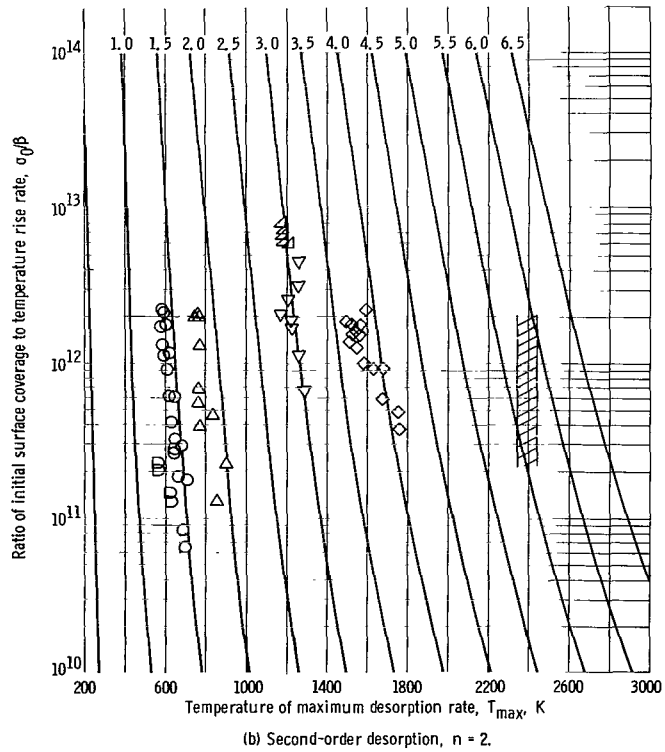

(b) Second-order desorption, n = 2.

Figure 5. - Temperature at which maximum desorption rate occurs for constant energy surface.

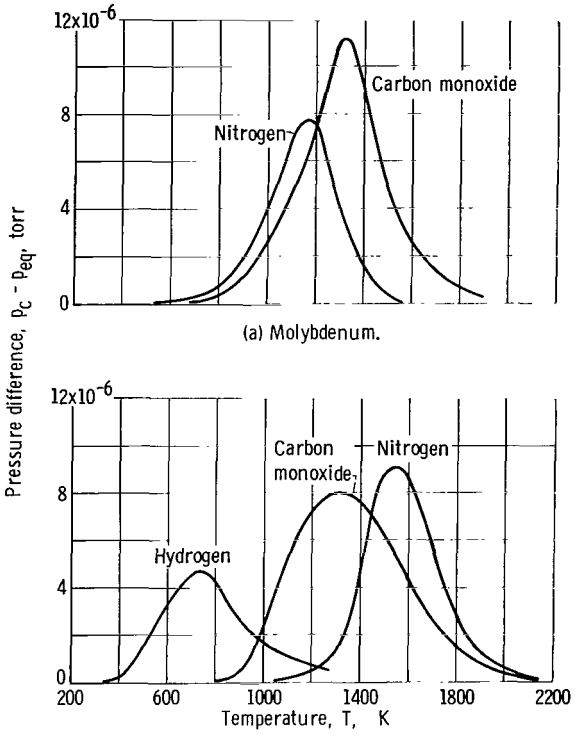

Figure 6. - Desorption curves for maximum coverage cases.

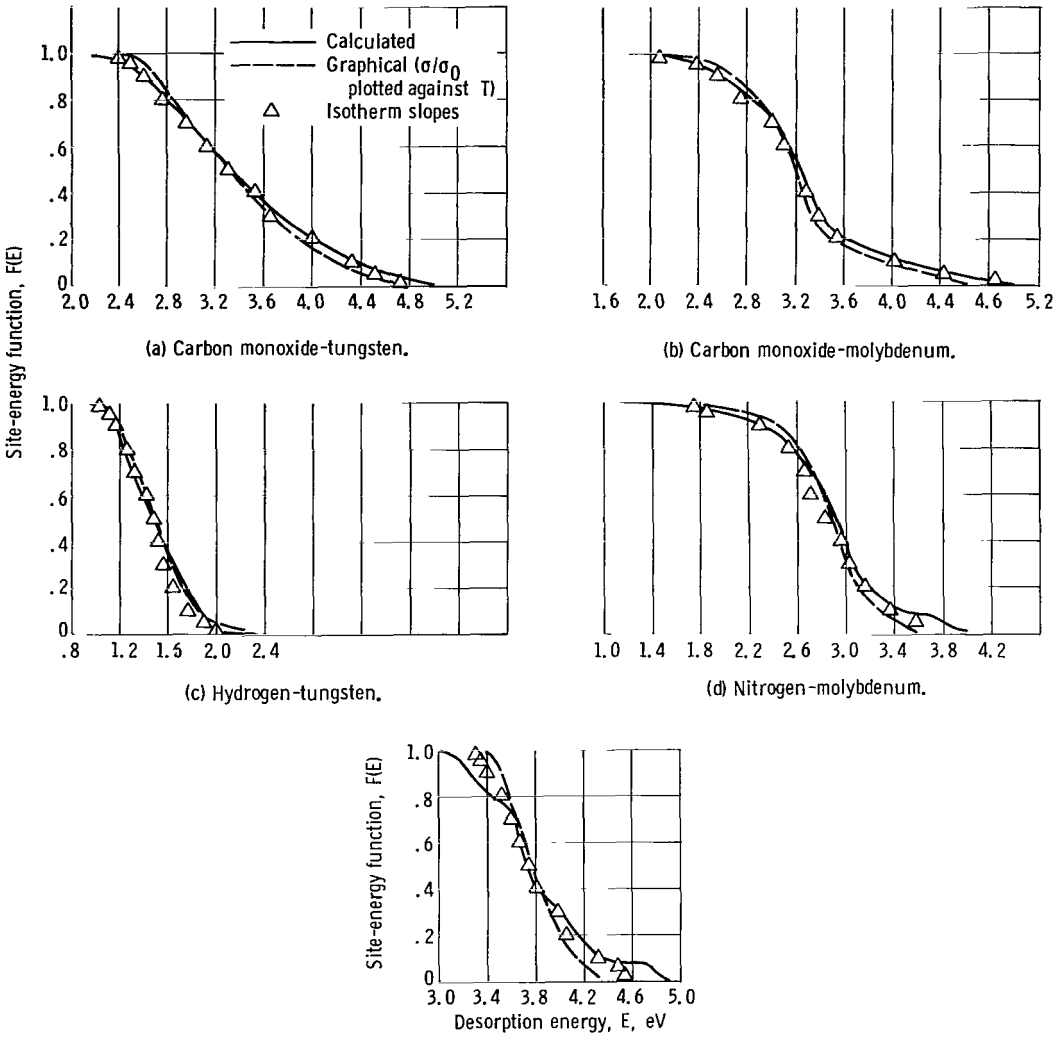

(a) Carbon monoxide-tungsten.

(b) Carbon monoxide-molybdenum.

(c) Hydrogen-tungsten.

(d) Nitrogen-molybdenum.

(e) Nitrogen-tungsten.

Figure 7. - Energy distribution function variation with energy.

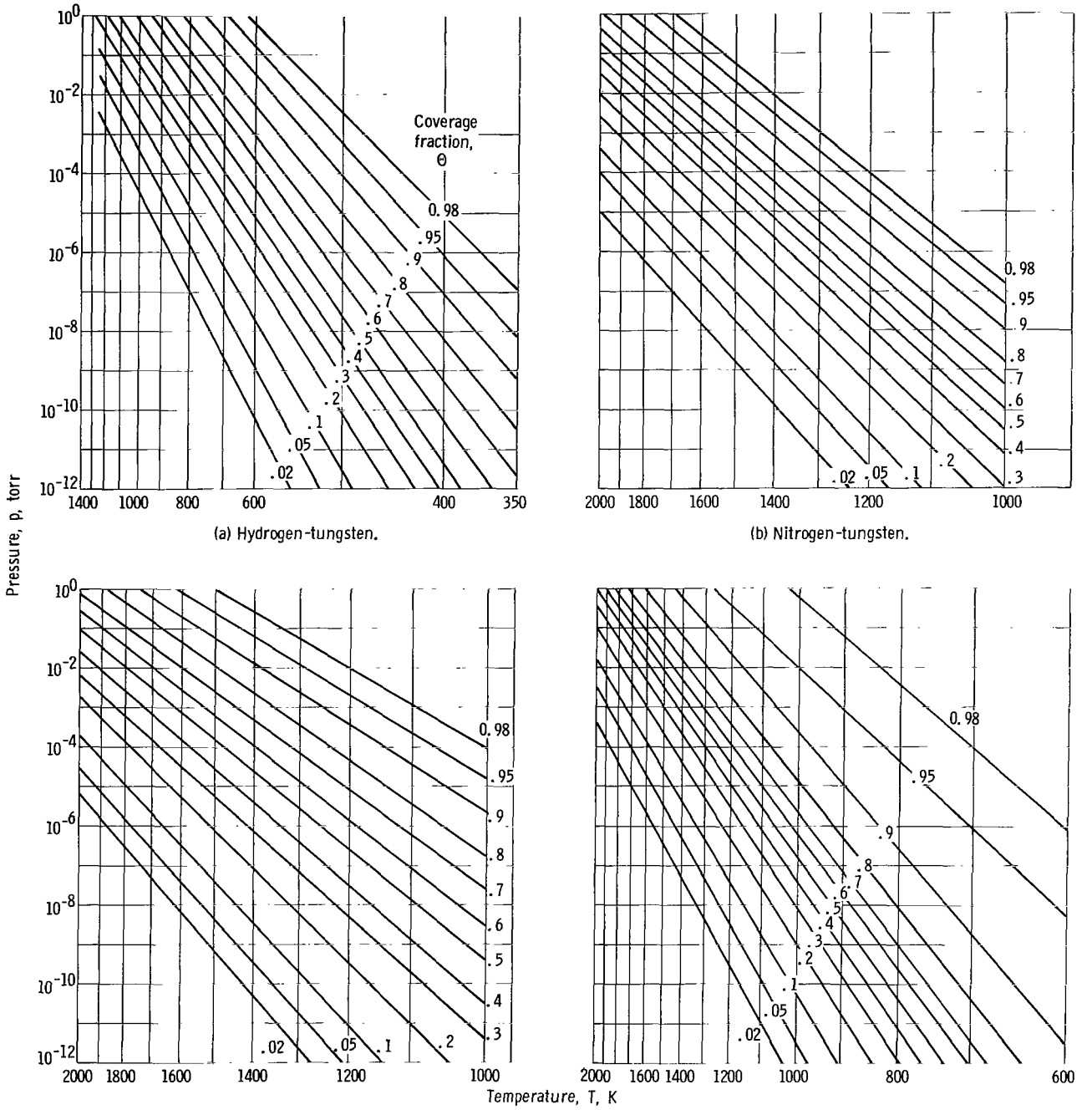

Figure 8. - Variation of equilibrium surface coverage with pressure and temperature for experimental heterogeneous surfaces.

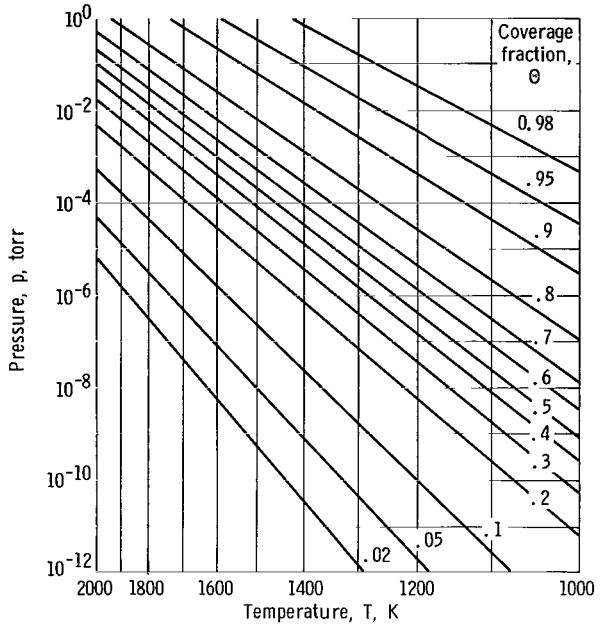

(e) Carbon monoxide-molybdenum.

Figure 8. - Concluded.

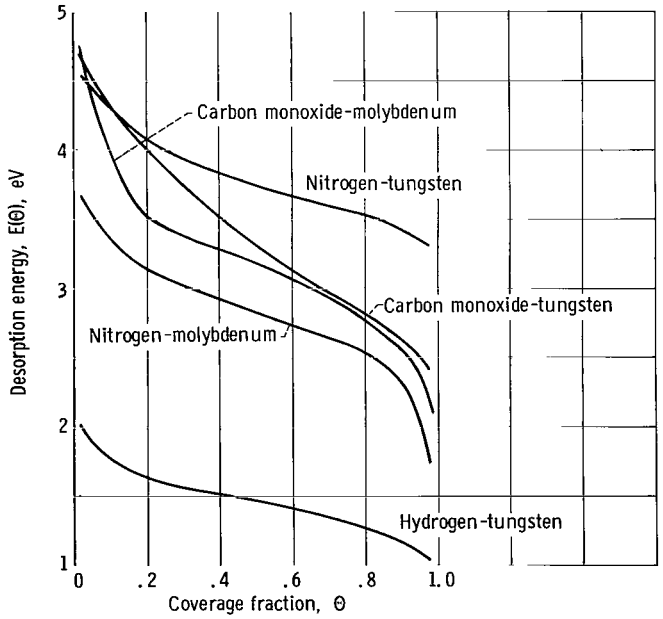

Figure 9. - Desorption energies determined from slopes of constant coverage lines of figure 8.

NATIONAL AERONAUTICS AND SPACE ADMINISTRATION
WASHINGTON, D. C. 20546

OFFICIAL BUSINESS

FIRST CLASS MAIL

POSTAGE AND FEES PAID
NATIONAL AERONAUTICS AN
SPACE ADMINISTRATION

POSTMASTER: If Undeliverable (Section 158
Postal Manual) Do Not Retur

"The aeronautical and space activities of the United States shall be conducted so as to contribute . . . to the expansion of human knowledge of phenomena in the atmosphere and space. The Administration shall provide for the widest practicable and appropriate dissemination of information concerning its activities and the results thereof."

—NATIONAL AERONAUTICS AND SPACE ACT OF 1958

NASA SCIENTIFIC AND TECHNICAL PUBLICATIONS

TECHNICAL REPORTS: Scientific and technical information considered important, complete, and a lasting contribution to existing knowledge.

TECHNICAL NOTES: Information less broad in scope but nevertheless of importance as a contribution to existing knowledge.

TECHNICAL MEMORANDUMS: Information receiving limited distribution because of preliminary data, security classification, or other reasons.

CONTRACTOR REPORTS: Scientific and technical information generated under a NASA contract or grant and considered an important contribution to existing knowledge.

TECHNICAL TRANSLATIONS: Information published in a foreign language considered to merit NASA distribution in English.

SPECIAL PUBLICATIONS: Information derived from or of value to NASA activities. Publications include conference proceedings, monographs, data compilations, handbooks, sourcebooks, and special bibliographies.

TECHNOLOGY UTILIZATION PUBLICATIONS: Information on technology used by NASA that may be of particular interest in commercial and other non-aerospace applications. Publications include Tech Briefs, Technology Utilization Reports and Notes, and Technology Surveys.

Details on the availability of these publications may be obtained from:

SCIENTIFIC AND TECHNICAL INFORMATION DIVISION

NATIONAL AERONAUTICS AND SPACE ADMINISTRATION

Washington, D.C. 20546